Open access • Journal Article • DOI:10.1007/S00339-016-0566-X

Characterization of Roman glass tesserae from the Coriglia excavation site (Italy) via energy-dispersive X-ray fluorescence spectrometry and Raman spectroscopy

Mary Kate Donais, Jolien Van Pevenage, Andrew Sparks, Monica Redente ...+4 more authors

Institutions: Saint Anselm College, Ghent University

Published on: 25 Nov 2016 - Applied Physics A (Springer Berlin Heidelberg)

Topics: Fluorescence spectrometry

Appl. Phys. A (2016) 122:1050
DOI 10.1007/s00339-016-0566-x

Applied Physics A
Materials Science & Processing

Characterization of Roman glass tesserae from the Coriglia excavation site (Italy) via energy-dispersive X-ray fluorescence spectrometry and Raman spectroscopy

Mary Kate Donais[1] · Jolien Van Pevenage[2] · Andrew Sparks[1] · Monica Redente[1] · David B. George[3] · Luc Moens[2] · Laszlo Vincze[2] · Peter Vandenabeele[4]

Received: 14 July 2016 / Accepted: 10 November 2016 / Published online: 25 November 2016

Abstract The combined use of handheld energy-dispersive X-ray fluorescence spectrometry, Raman spectroscopy, and micro-energy-dispersive X-ray fluorescence spectrometry permitted the characterization of Roman glass tesserae excavation from the Coriglia (Italy) archeological site. Analyses of ten different glass colors were conducted as spot analyses on intact samples and as both spot analyses and line scans on select cross-sectioned samples. The elemental and molecular information gained from these spectral measurements allowed for the qualitative chemical characterization of the bulk glass, decolorants, opacifiers, and coloring agents. The use of an antimony opacifier in many of the samples supports the late Imperial phasing as determined through numismatic, fresco, ceramics, and architectural evidence. And dealinization of the exterior glass layers caused by the burial environment was confirmed.

1 Introduction

Glasses are commonly found within archeological excavation sites in various forms from large vessels to jewelry to small tesserae cubes used to construct mosaics [1–4]. Chemically composed of mostly silica from sand, additional substrates such as sodium carbonate (soda) or natron (hydrated sodium sulfate mixed with sodium bicarbonate and other minor components) were added to the silica as fluxing agents to lower the melting temperature and increase the time to solidify. Lower concentration species such as impurities in the bulk raw materials, opacifiers, decolorants, and coloring agents are also present; these contribute to the physical characteristics and visual appearance of the glasses [4–6]. Additionally, trace element concentrations within sands and glasses can be used to investigate regional variations and artifact provenance [1, 7, 8].

Considering the many species present in glasses, a wide range of analytical techniques are available for their characterization. Recent examples include X-ray fluorescence spectrometry [9–12], Raman spectroscopy [12, 13], inductively coupled plasma mass spectrometry [1], laser ablation inductively coupled plasma mass spectrometry [7, 14, 15], inductively coupled plasma atomic emission spectroscopy [2], scanning electron microscopy with energy-dispersive X-ray spectroscopy [3, 7, 11, 16], X-ray photoelectron spectroscopy [10], particle-induced X-ray/gamma ray emission [3, 10], laser-induced breakdown spectroscopy [17, 18], electron microprobe analysis [16, 19], and X-ray powder diffraction [16]. Some of these studies were conducted with portable instrumentation, thus permitting on-site and/or in situ analyses of the artifacts [9–13, 20]. And most research campaigns utilized multiple, complimentary techniques to more completely characterize and understand the materials.

The glass tesserae explored for this study were found at the Coriglia, Castel Viscardo excavation site located approximately 13 km northwest of Orvieto, Italy. Excavations at this site have been conducted since 2006 under

✉ Mary Kate Donais
mdonais@anselm.edu

[1] Department of Chemistry, Saint Anselm College, 100 Saint Anselm Drive, Manchester, NH, USA

[2] Department of Analytical Chemistry, Ghent University, Krijgslaan 281, S12, Ghent, Belgium

[3] Department of Classics, Saint Anselm College, 100 Saint Anselm Drive, Manchester, NH, USA

[4] Department of Archaeology, Ghent University, Sint-Pietersnieuwstraat 35, UFO, Ghent, Belgium

the auspices of the Soprintendenza per I Beni Archeologici dell'Umbria and the Parco Archaeologico e Ambientale dell'Orvietano. Under the direction of David George and Claudio Bizzarri, many artifact types from Coriglia have been identified and chemically analyzed including mortars [21], hydraulic cements [21], hypocaust tiles [22], and fresco pigments [23]. The site at Coriglia has a long history. It has yielded evidence of occupation from at least the eighth-century BCE to the sixteenth-century CE with structures dating from the Archaic Etruscan phase in the sixth-century BCE until a fourteenth-century CE phase of medieval reuse and repurposing of a series of late Roman Imperial structures. The Roman Imperial phase had monumental structures [24].

The most visually striking aspect of the site is a series of Roman structures dating from the Republic to Late Empire that were dedicated to the use of water. In the upper part of the site, there are a number of large vascae that were likely intended to create head water for a very large bath complex 150 m down a slope created by a series of terrace walls. There is evidence for the existence of bath complexes on the site from the late Republican period at the end of the first-century BCE through the fourth-century CE. The Imperial period bath complex was quite well appointed with marble imported from Anatolia as well as North Africa. The tesserae examined in this paper came from the context of this bath and are probably from the Imperial phase.

Energy-dispersive X-ray fluorescence (EDXRF) spectrometry was chosen for the initial glass studies based on the valuable elemental information that this technique can convey for glasses and its proven utility from previous research in the field [9–11, 25, 26]. Additionally, by using a handheld EDXRF for the work, the applicability of this instrument for field-based data collection could be demonstrated. Through collaborations with researchers at Ghent University, additional analyses of the glasses using Raman spectroscopy and micro-EDXRF spectrometry were then conducted. The complimentary molecular information provided via Raman analysis allowed for a stronger understanding of the glasses' compositions. And the line scans via both Raman and micro-EDXRF permitted additional material characterization and exploration of compositional variations between the outer and inner portions of the tesserae.

2 Experimental method

2.1 Glass tesserae samples

Glass tesserae were unearthed at the Coriglia excavation site in 2009. The tesserae are all approximately cubical in shape with dimensions ranging from 6 to 15 mm on each side. The samples were cleaned with water and a soft brush to remove dirt from the exterior. Visual inspection permitted classification into ten groups by color: aqua, teal, translucent blue, light blue, dark blue, red, black, translucent green, light green, and dark green. The aqua, teal, clear blue, light blue, and dark blue are all considered to fall within the general blue category, whereas the clear green, light green, and dark green are all considered to fall within the green category. All colors not labeled as translucent were opaque. Figure 1 provides representative examples of the ten tesserae colors with a scale to estimate size.

Initial studies on the glasses were performed on these manually cleaned glasses. Tesserae were examined as intact samples via both EDXRF spectrometry and Raman spectroscopy. Additionally, a select small sample set of tesserae were cross-sectioned and examined via both Raman and micro-EDXRF to evaluate homogeneity and elemental enrichment/depletion at the sample exterior compared to the interior bulk glass. These line scans were performed on a "fresh" cross section of each tesserae sample, so minimal sample preparation was needed. A diamond saw was used for this purpose. After cutting, the surface was cleaned with demineralized water.

2.2 Handheld EDXRF spectrometry

EDXRF data were collected with two different instruments: (1) a Bruker Tracer III-SD instrument (Kennewick, WA, USA) with a silicon drift detector and a Rh target X-ray tube excitation source which was operated under vacuum conditions at 15 kV with a beam current of 25 μA and no filter; and (2) a Bruker Tracer III-V + instrument (Kennewick, WA, USA) with a SiPIN detector and a Rh target X-ray tube excitation source but instead operated under atmospheric conditions at 40 kV with a beam current of 25 μA and the yellow filter composed of 0.001 in Ti and 0.12 in Al. Both instruments have an elliptical spot size of approximately 3/4 mm (9.4 mm^2). The instruments were operated in benchtop mode with the stand and cover using power supplied from a wall outlet and a laptop computer for instrument control and data storage. Data were collected for some but not all tesserae colors with the former instrument in triplicate for 150 s each on multiple spots for each sample, whereas all other handheld EDXRF data were collected with the later instrument for 120 s in either duplicate or triplicate on multiple spots for each sample. Under these two sets of EDXRF instrument conditions, elements from aluminum ($Z = 13$) to lead ($Z = 82$) were detected.

Fig. 1 *Top row* (l-r) aqua, teal, translucent *blue*, *light blue*, *dark blue*; *bottom row* (l-r) *red*, *black*, *translucent green*, *light green*, *dark green*

2.3 Raman spectroscopy

The Raman measurements were executed with a Bruker Senterra R200-L Raman spectrometer (Brussels, Belgium). This spectrometer is equipped with two lasers: a red diode laser (785 nm) and a green Nd:YAG laser (532 nm). The spectrometer is equipped with a thermoelectrically cooled CCD (1024 × 256 pixel), two gratings, a filter changer consisting of Rayleigh filters, a ND filter wheel for changing the laser power, a slit-type aperture, and a pin-hole-type aperture.

For the analyses of whole uncut tesserae, each was put as such in the instrument. Before measuring, the surface was cleaned with demineralized water. In this project, both the red diode laser (785 nm) and the green Nd:YAG laser (532 nm) were used. The laser power and the measurement time varied between 2.57 and 25.9 mW and 150 and 2700 s, respectively. The spot size was <10 μm. At least three different spots were measured on each sample.

For the analyses of the sectioned tesserae, an autofocus was performed before each measured spot. Both the red and green lasers were used with a power varying between 2.57 and 25.9 mW. The spot size of the laser beam on the sample is <10 μm. The measurement time on each spot varied between 150 and 600 s.

2.4 Micro-EDXRF spectrometry

Micro-EDXRF measurements were taken with the EDAX Eagle-III instrument (Mahwah, NJ, USA). This spectrometer is equipped with a micro-focus X-ray tube with a Rh anode and a liquid-N_2-cooled 80-mm^2 energy-dispersive Si-(Li) detector. In the sample chamber, the samples are positioned using an XYZ motorized stage and a high-resolution microscope, and the X-rays are focused using an X-ray Optical Systems Inc. polycapillary lens (East Greenbush, NY, USA). Because the measurements are taken in vacuum, the Rh-L photons originating from the X-ray tube can be used to improve the sensitivity of low Z-elements down to sodium (Na). The parameters used during the line scans were as follows: 40 kV X-ray tube voltage, 25–80 μA current, 150 s live time, ~30% dead time, and a 150-μm-diameter spot size. The analyzed length of the line scan was typically 3 mm with a 143-μm step size.

3 Results and discussion

In the following, for each color category of glasses, the EDXRF and Raman results are shown and discussed. The elements and structural features indicative of the bulk glass are summarized and discussed in Sect. 3.6.

Analyses by handheld EDXRF permitted quick and straightforward determination of the detectable elements present in the glasses. The elements identified in the glasses included aluminum (Al), silicon (Si), calcium (Ca), titanium (Ti), manganese (Mn), iron (Fe), nickel (Ni), copper (Cu), lead (Pb), strontium (Sr), tin (Sn), and antimony (Sb). Representative EDXRF spectra collected via the handheld instrument under atmospheric conditions for each tesserae color are provided on a single set of axes for ease of comparison in Fig. 2; intensities were adjusted to the rhodium Compton peak in each spectrum. Some elements such as titanium and nickel were positively identified in samples, but at such low levels that their signals are not visible in the spectra in Fig. 2. The EDXRF spectra collected under vacuum conditions showed very few differences among the glass colors examined; these spectra are not included in this paper for space considerations.

Analyses of the intact, whole tesserae via Raman spectroscopy proved challenging and yielded few if any conclusive results for a number of the samples. Spectra collected on the cross-sectioned samples were more

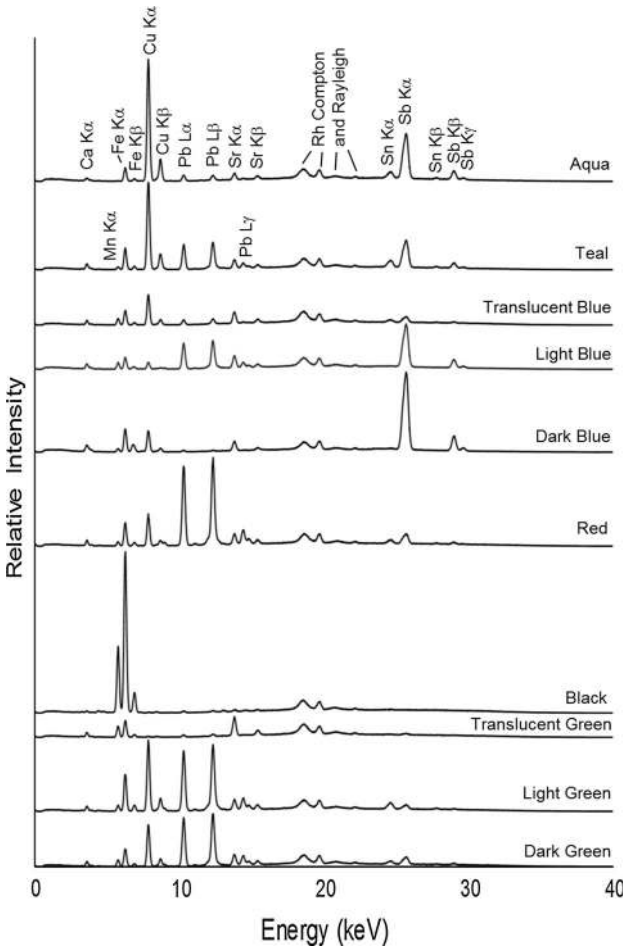

Fig. 2 Representative XRF spectra of the ten glass *tesserae colors*

encouraging, however, and allowed for the identification of bands for many of the colors including dark blue, red, black, and dark green.

3.1 Blue tesserae

In Fig. 2, it can be observed that clearly detectable lower levels of calcium, iron, and strontium were found in all the blue tesserae samples. In addition, the aqua, teal, and translucent blue glasses exhibited high levels of copper and low but clearly detectable levels of antimony and tin. In contrast, the light blue and dark blue tesserae had lower levels of copper and higher levels of antimony compared to the other blue tesserae and no detectable tin. The copper present in all the blue glass samples is expected as this element contributes to their blue color [27]. Lead levels varied considerably among all the blue glass colors and even within each color grouping; this was especially evident among the dark blue tesserae with some samples at very low levels as depicted in the XRF spectrum in Fig. 2 and others at much higher levels as has been previously reported [28]. This observation leads one to hypothesize that the blue glass samples are of two types: a silica-soda-lime type and a silica-soda-lime-lead oxide type as has been previously reported for Roman glasses [29]. The manganese found in the translucent blue glasses is most likely acting as a decolorant [27], whereas its antimony level, the lowest of all the blue glasses, is supported visually by its non-opaque character [5].

Different Raman bands appear in the spectra measured on the surface of the aqua sample (Fig. 3a). Some bands can be identified, others not. The bands positioned at 235, 440 (under 463 cm^{-1}), and 614 cm^{-1} might be from rutile (TiO_2) [30]. The band at 235 cm^{-1} on the other hand can also be from $CaSb_2O_6$, together with the band at 463 and 669 cm^{-1} [31]. The band at 516 cm^{-1} is not identified, but as it is a rather broad band, it is probably a dissolved feldspar. The broad band at 1087 cm^{-1} can be attributed to ν_{max} Si–O vibrations of soda-lime glasses [32]. The sharp band at 659 cm^{-1} is not identified. Although a high copper signal was detected via XRF, no copper-containing pigment could be detected. Possibly, the pigment decomposed on heating at the glass melting temperature. The band at 994 cm^{-1} will be discussed in Sect. 3.6.

Different components are identified by the Raman measurements on the teal tesserae as shown in Fig. 3b. The bands at 551 and 1097 cm^{-1} are the δ_{max} Si–O and ν_{max} Si–O vibrations of soda-lime glasses, respectively [32]. The Raman bands at 237 and 671 cm^{-1} can be attributed to $CaSb_2O_6$ [31] and are supported by the XRF spectral results. The band at 995 cm^{-1} is discussed in Sect. 3.6. In another spot, calcite ($CaCO_3$) also was detected, showing bands at 150, 279 and 1085 cm^{-1} [33].

In a red/brown spot in the translucent blue sample, typical bands of an iron oxide structure (haematite, α-Fe_2O_3) appear at 220, 289, 398 and 1317 cm^{-1} [34, 35] as shown in Fig. 3c. The bands at 148, 199, 398, 507 and 631 cm^{-1} can be attributed to anatase (TiO_2) [36]. The presence of iron and titanium in the translucent blue glass is supported by the XRF spectral data in Fig. 2. Lead and manganese also were noted in the XRF spectra of the translucent blue glass. As has been previously reported for Roman translucent blue glasses, lead is acting as a chromophore and manganese as a decolorant [29].

No informative spectra were obtained from the spot measurements on the surface of the dark blue whole tesserae. But, measurements on the cross section of the sample when performing Raman line scans provided indicative data. One spectrum is shown in Fig. 3d. In this spectrum, both Raman bands of $CaSb_2O_6$ and $Ca_2Sb_2O_7$ are observed at 237, 337, 671 and 325, 478, 633, 790 cm^{-1}, respectively [31]. The Raman band at 145 cm^{-1} is identified as a Pb–O stretching vibration [31], while the broad bands at 547 and 1090 cm^{-1} can be attributed to δ_{max} Si–O and ν_{max} Si–O vibrations of soda-lime glasses

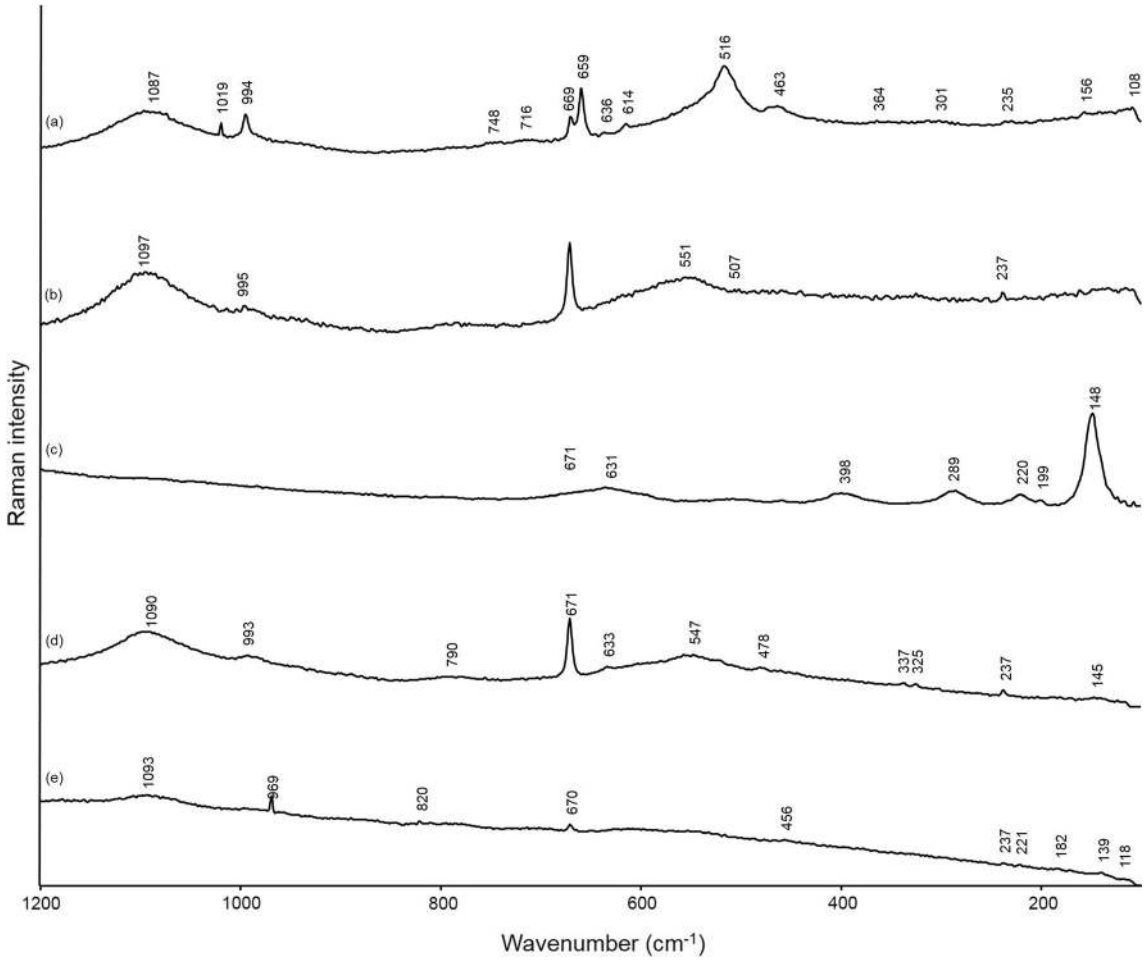

Fig. 3 Representative Raman spectrum for **a** *aqua tesserae* indicating the presence of rutile (TiO_2), $CaSb_2O_6$, and dissolved feldspar; **b** *teal tesserae* indicating the presence of $CaSb_2O_6$; **c** a *red/brown spot* in the translucent *blue glass* tesserae indicating the presence of haematite (α-Fe_2O_3) and lead tin antimonite ($Pb_2Sb_{2-x}Sn_xO_{7-x/2}$); **d** *dark blue tesserae* indicating the presence of $CaSb_2O_6$, $Ca_2Sb_2O_7$, and Pb–O stretching; **e** a *blue spot* in the *light blue glass tesserae* indicating the presence of $Pb_2Sb_2O_7$ and $Ca_2Sb_2O_7$

[32]. The detection of calcium, antimony, and lead in the dark blue tesserae via XRF analysis supports the Raman data.

Additionally, the components in the light blue tesserae are similar to those detected in the dark blue tesserae as already observed in the XRF spectral discussion earlier in this paper. In the light blue tesserae, both brown and blue particles were also visible under the microscope. In the brown particle, calcite ($CaCO_3$) was detected with Raman bands at the positions 281 and 1085 cm^{-1} [37]. In the blue particle, mixtures of different components were identified. The bands at 139 and 456 cm^{-1} show the presence of $Pb_2Sb_2O_7$ [32]. Further, the bands at 237 and 670 cm^{-1} can be identified as $Ca_2Sb_2O_7$ [32]. The band at 969 cm^{-1} will be discussed in Sect. 3.6. A Raman spectrum of the blue particle in the light blue tesserae is shown in Fig. 3e.

For the dark blue tesserae examined as a cross section via micro-EDXRF, a small change in intensity can be noticed when comparing the first spectrum, a spectrum taken in the middle of the line scan, and last spectrum. As shown in Fig. 4a, the peaks have a higher intensity at the outer part of the sample, compared to the inner part, and therefore indicate an enrichment in these elements at the glass surface. This small change in intensity can also be seen in the result from the line scan shown in Fig. 4b: Lead, antimony, zinc, copper, cobalt, iron, manganese, calcium, and potassium show a higher intensity at the beginning of the line scan and decrease after three measured spots (which is after about 430 µm) to remain stable till the end of the line scan in the glass interior. The red line in Fig. 4b indicates where this decrease in intensity was observed. Note that cobalt was found via the micro-EDXRF analyses but not with the portable EDXRF; the very low amounts of cobalt necessary to impart a blue color to glass, often <0.05%, can be below EDXRF detection limits [29].

The results from the Raman line scans are shown in Fig. 5. Different bands were integrated as specified on the

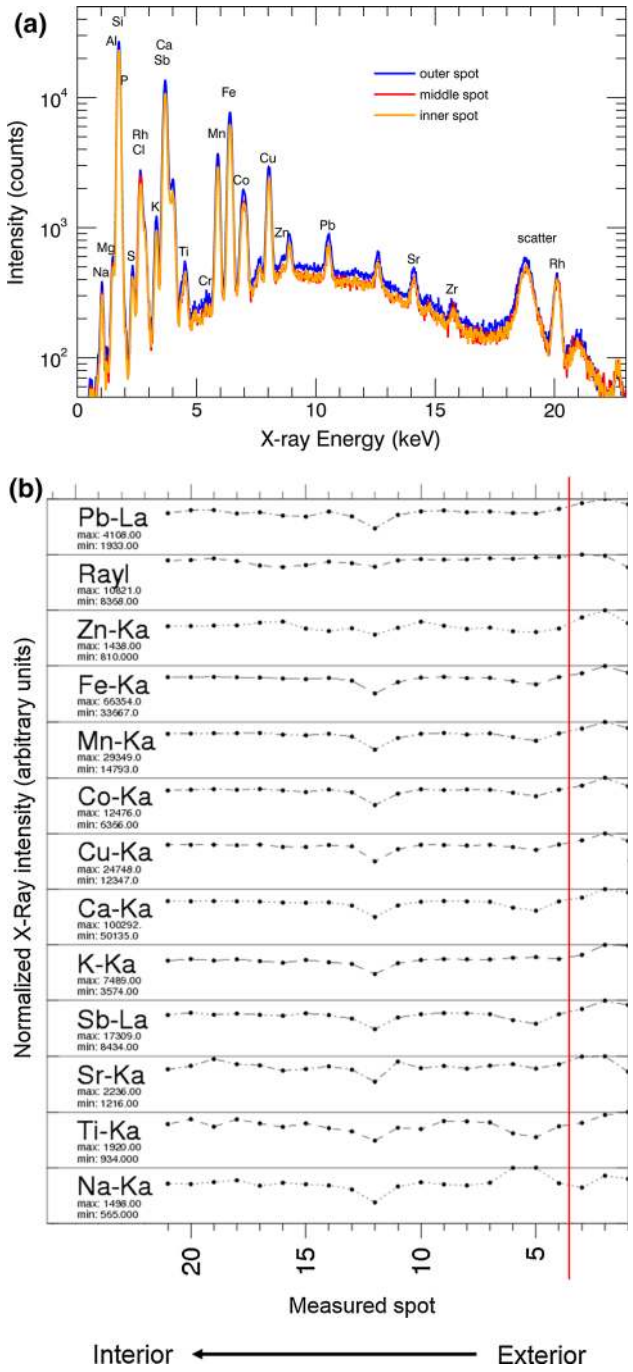

Fig. 4 **a** Comparison of micro-XRF spectra from the outer, middle, and inner areas of the *dark blue* cross-sectioned tesserae, **b** micro-EDXRF line scan from exterior (r of graph) to interior of *dark blue tesserae*

figures: ca. 140, 480, 633, 670, 993 cm^{-1} and are discussed below. As was discussed earlier in Sect. 3 and noted in Fig. 3d, the Raman band around 140 cm^{-1} can be identified as a Pb–O stretching vibration [38]. Except for the last spot of the Raman line scan, a gradual decrease in intensity is observed for this Raman band moving from the exterior to the interior of the tesserae (Fig. 5a). These Raman

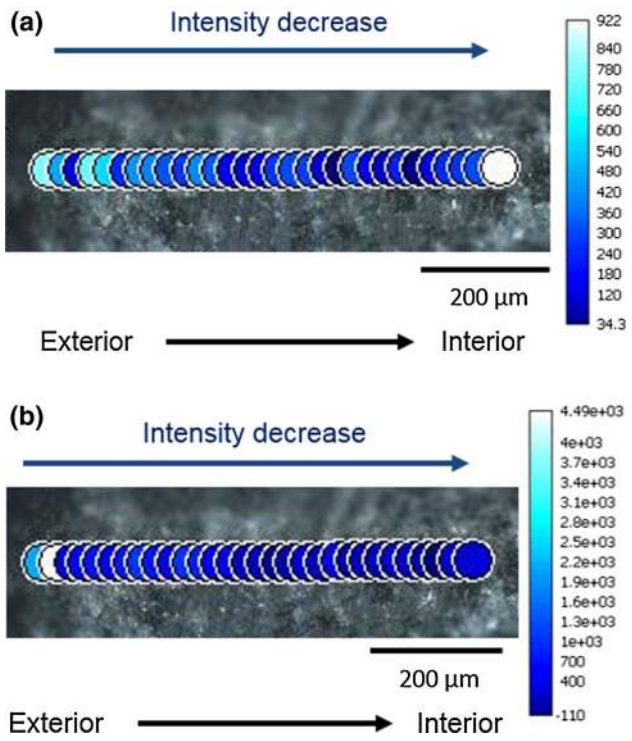

Fig. 5 Raman spectroscopy line scan from exterior (l of figure) to interior of the *dark blue tesserae* with integrated Raman band results from **a** 146 to 127 cm^{-1} and **b** 498 to 464 cm^{-1}

results agree somewhat with the micro-EDXRF; the micro-EDXRF intensities for lead were higher at the sample surface compared to the interior, but this was only found for the first few spots and did not continue gradually as was the observed trend in Raman signal. The Raman bands at position 480, 633 and 670 cm^{-1} that were identified as $Ca_2Sb_2O_7$ and $CaSb_2O_6$ [32], respectively, show a higher intensity at the outer side of the sample compared to the inner part, but no gradual decrease in intensity is observed moving toward the inner part of the sample. These results, as shown in Fig. 5b for integration of the 480 cm^{-1} band, are in agreement with the micro-EDXRF results.

3.2 Red tesserae

Red is a more rare glass color compared to the other glass colors found at the Coriglia site. The few samples that have been analyzed contain significant levels of lead and lower levels of copper and iron. Previously reported analyses of red glasses document two types, one containing copper (I) oxide as the species imparting the red color and another containing micron droplets of metallic copper. In either instance, these studies support our finding of copper [27, 39, 40] as shown in Fig. 2.

Different spot measurements were executed on the surface of the red tesserae. Unfortunately, the component that

contributes the red color to this glass could not be identified by the Raman measurements. Previous investigations on red Roman glasses show that the collection of Raman spectra is difficult because of the light absorption of Cu^0 particles [41, 42]. However, two Raman bands can be observed. The band around 143 cm^{-1} can be identified as a Pb–O vibrational mode [38]. Further, an additional band at 97 cm^{-1} appears and can be identified as a ternary oxide-based phase of the Pb–O stretching mode [38]. These results agree with the elevated lead levels observed in the EDXRF spectra for the red tesserae. In one of the spectra of the line scans, an additional band was noticed at 513 cm^{-1}. This band might be explained as bindheimite ($Pb_2Sb_2O_7$) [32], but because no Sb was detected by the XRF measurements, it might originate from anatase (TiO_2), which has vibrational modes at 146, 513 and 636 cm^{-1} [43]. This last vibrational mode (at 636 cm^{-1}) was not observed in the spectrum, however. Upon this observation, the XRF spectra for the red tesserae were examined, and there is very low titanium present in the samples, which could provide a sufficient Raman signal for anatase as it is a strong Raman scatterer.

No significant differences in elemental composition were found when comparing the micro-EDXRF spectra from the interior and exterior of the red tesserae. Moreover, no clear trend in terms of increase or decrease in intensity of the observed Raman bands was found when moving from the outer to the inner part of the sample.

3.3 Black tesserae

Black tesserae are also rare glass colors of all those found at Coriglia. The two major elements identified in the black glasses are manganese and iron with low levels of lead. Manganese is commonly used in the preparation of purple glass, thus indicating that our black glass is in reality a very dark purple. This observation is supported by previously reported findings on black-appearing Roman glasses [7, 44].

In a red/brown spot in the black tesserae, different components are detected. Quartz shows bands at 125, 205, and 463 cm^{-1} [45]. Goethite (FeO(OH)) shows bands at 245, 299, 396 and 549 cm^{-1} [43]. Because goethite should have been destroyed at the glass formation temperature, it is probably a contamination on the surface of the sample. However, from the Raman line scan on the cross section of the sample, magnetite (Fe_3O_4) was detected with a strong, broad band at 660 cm^{-1}. The Fe_3O_4 spinel or Co-, Cr-, Zn-substituted homologues were also reported as a pigment for black beads in a study of glass trade beads by Prinsloo et al. [46]. The EDXRF spectral data indicating the presence of iron support the Raman findings. In the literature, also Fe–S chromophores are reported to produce black beads [47, 48]. Although the position of the Raman bands of Fe–S chromophores varies in shape and wavenumber position, no similar spectrum was recorded in this study.

The micro-EDXRF line scans on the black tesserae showed varying patterns for the elements with no observable trend. Magnetite (Fe_3O_4) was also detected via Raman line scans together with the Pb–O vibration. The intensity of these two bands was found to be higher at the outer side of the sample compared to the interior of the sample.

3.4 Green tesserae

The light green and dark green tesserae have virtually identical EDXRF spectra with high levels of iron, copper, and lead and lower levels of calcium, manganese, strontium, and zirconium. The translucent green tesserae also have elevated iron together with elevated manganese and strontium compared to their lower levels of calcium and lead. The copper identified in the light and dark greens is consistent with previously studied green glasses [17]. However, the lack of copper in the translucent green tesserae suggests that these samples might better be described as "white" and not green. The higher manganese found in the translucent green samples indicates that it was likely acting as a decolorant [27]. And similar to that observed for the blue tesserae, the light green and dark green glasses exhibited a wide range of lead levels within their color groupings.

Bindheimite ($Pb_2Sb_2O_7$) was detected in the light green tesserae with Raman bands positioned at 141, 338, 458 and 512 cm^{-1} [32]; the presence of bindheimite in Roman glasses from the third- and fourth-century CE has been previously reported but identified instead via X-ray diffraction [29]. The broad band at 1090 cm^{-1} can be attributed to ν_{max} Si–O vibrations of soda-lime glasses [32]. The band at position 994 cm^{-1} is discussed in Sect. 3.6. Two differently colored spots were observed in the dark green tesserae, one green and one dark red. The Raman spectrum from the green spot showed broad bands related to the glass structure (at 553 and 1096 cm^{-1}), and the band at 988 cm^{-1} is discussed in Sect. 3.6. In a dark red spot of the dark green tesserae, calcite was detected with Raman bands positioned at 277 and 1085 cm^{-1}.

The results of the micro-EDXRF line scans of the dark green tesserae showed no clear difference in peak intensities between the inner and the outer spots. However, having a closer look at the horizontal plot of the line scan, it can be seen that there is a "large" decrease in intensity for iron, titanium, potassium, aluminum, and magnesium; a "small" decrease for lead, strontium, and manganese; and an increase for sodium moving from the outer part to the inner part of the sample. These micro-EDXRF results are shown in Fig. 6 with a vertical red line indicating where the intensities decrease; elements with "large" decreases are

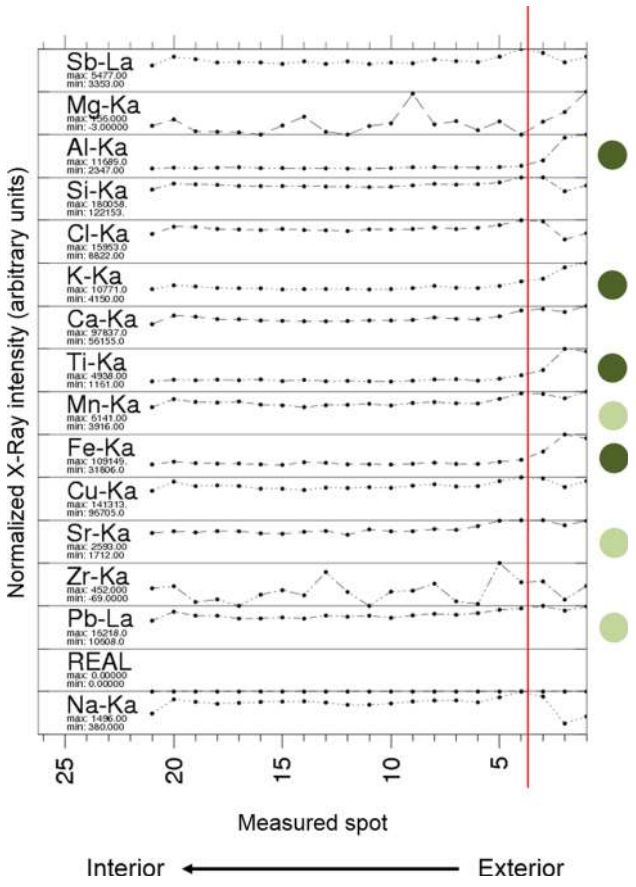

Fig. 6 Micro-EDXRF line scan from exterior (r of graph) to interior of the *dark green tesserae*

indicated with a dark green spot and those with "small" changes are indicated with a light green dot. Also for the Rayleigh peak, a small decrease in intensity is observed. This might be due to a change in composition of the matrix. Because not all detected elements follow the same trend, their observed decrease in intensity was probably due to a change in matrix composition and not due to the elemental source itself.

The Raman spectra of the dark green tesserae show typical bands of a lead–tin antimonite ($Pb_2Sb_{2-x}Sn_xO_{7-x/2}$) [31]. Also, the band at 987 cm^{-1} can be observed in the spectrum. The appearance of this band and its identification will be discussed in §3.6. Integration of this band showed no particular increase or decrease in intensity when moving over the surface of the sample.

3.5 Summary of observations

A table summarizing our qualitative assessment of the handheld EDXRF data collected under atmospheric conditions is provided as Table 1. All signals at 10% or higher compared to the largest peak for that tesserae color are labeled as high (H), and all other observable peaks are considered low (L). Any elemental peak with a signal-to-noise ratio less than 3.0 was considered non-detected (ND). Note that these designations do not represent relative concentrations as this was a qualitative study only. Any elements found at both high and low signals in different samples within that color grouping are indicated as such with a H/L designation in the table. Any elements found at both low and non-detected signals in different samples are indicated as such with a L/ND designation in the table. Combining these results with the vacuum conditions portable EDXRF and micro-EDXRF results, common elements indicative of the bulk glass were identified as sodium, potassium, aluminum, silicon, calcium, titanium, iron, lead, and strontium. Sodium was found in all glass colors but black. And as was noted specifically for some of the blue glasses, lead was found at high levels in some samples but was low in others.

Despite the color differences of the glasses, similar Raman bands appeared in the Raman spectra. An overview of the different phases is given in Table 2. In many cases, a Raman band between 970 and 995 cm^{-1} is observed. This band was also observed by Colomban et al. [49] both in green and in blue mosaics, but also in colorless and pale-yellow mosaics. He also mentioned the presence of the band but could not explain it. In a later study, Ricciardi et al. [32] observed a band around 995 cm^{-1} during the investigation of Roman Age mosaic glass tesserae and assigned it to a calcium and/or aluminum–silicate, incorporating cobalt ions. In the same study, it is suggested that the Raman signature corresponds to alkali sulfates, glaserite $(K_2)^{2+}(KNa)^{2+}(SO_4)_2^{4-}$ being the model compound, in which a partial substitution with Co may be possible. In this study, from the EDXRF measurements we can observe that cobalt was not present, or only in very small amounts making it not detectable.

For the dark blue and dark green tesserae examined via EDXRF and Raman spectroscopy line scans, a depletion in Na in the outer layer was found for the dark green and dark blue tesserae. This observation is supported by previous studies on glass deterioration, which report dealinization in the outer glass layers and specifically in sodium and calcium [17, 50–53]. The loss of alkalis and resulting decay of the glass' exterior layer are attributed to exposure to aqueous environments during burial, which is enhanced under acidic conditions. The observed higher levels of calcium and potassium in the dark blue and dark green tesserae appear to contradict the observed Ca depletion, however. An explanation for the enhanced levels of the minor elements (lead, antimony, zinc, copper, cobalt, iron, manganese, titanium) is also challenging considering the qualitative nature of the measurements. With some of the major glass elements depleted, the enhanced minor element signals may be a result of a positive attenuation due to the changed outer layer matrix.

Table 1 Overview of EDXRF results by color and element

Tesserae	Calcium (Ca)	Titanium (Ti)	Manganese (Mn)	Iron (Fe)	Nickel (Ni)	Copper (Cu)	Lead (Pb)	Strontium (Sr)	Tin (Sn)	Antimony (Sb)
Aqua	L	L	L	H	ND	H	L/H	H	L	H
Teal	L	L	ND	H	ND	H	L/H	H	L	H
Translucent blue	H	L	H	H	ND	H	H	H	L	H
Light blue	H	L	H/L	H	L	H	H	H	L	H
Dark blue	H	L	H/L	H	L/ND	L	L/H	H	ND	H
Red	H	L	L	H/L	ND	H	H	L	L/ND	L/ND
Black	L	L	H	H	ND	L/ND	L/ND	L	ND	ND
Translucent green	H	ND	H	H	ND	L	L	H	ND	L
Light green	L	L	L	H	ND	H	H	H	L	L
Dark green	L	L	H	H	ND	H	H	H	L/ND	L

H high, *L* low, *ND* non-detected

Table 2 Overview of Raman results by color and identified phases

Tesserae	Pb–O vibrational mode (144 cm^{-1})	$Pb_2Sb_2O_7$	$CaSb_2O_6$	$Ca_2Sb_2O_7$	δ_{max}Si–O vibrations of soda-lime glasses	ν_{max}Si–O vibrations of soda-lime glasses	Calcite	Rutile	Iron oxide	Orthoclase	Quartz	Alkali sulfates
Red	×	×										
Aqua			×			×		×				×
Teal			×		×	×	×					×
Trans. blue		×			×	×		×	×			
Light blue							×					×
Dark blue	×		×	×	×	×						
Red	×	×										
Black									×		×	
Trans. green												
Light green		×				×						×
Dark green					×	×	×					×

4 Conclusions

The use of EDXRF in both a portable instrument and micro-instrument configuration, together with Raman spectroscopy, proved to be an informative first step in characterizing Roman glasses from the Coriglia excavation site. Antimony and not tin was used as the opacifying agent in most of these glasses. A shift from antimony-based opacifiers to tin-based opacifiers occurred in the fourth-century AD [54], so therefore the Coriglia glasses predate that period. Phasing of the site based on numismatic, fresco, ceramics, and architectural evidence supports this conclusion in that the area where the tesserae were found is likely late Imperial.

Cross sectioning of samples followed by line-scan analyses proved advantageous and necessary to obtain quality data for both the micro-EDXRF spectrometry and Raman spectroscopy work. This is likely due to corrosion layers on sample exteriors caused by the burial environment at the excavation site. Chemical differences between

the exterior corrosion layer and interior bulk glass were determined to be dealinization likely caused by exposure to water.

Additional work is clearly needed and planned. A high priority is to expand the specimen set to include more samples per color group and could even reveal additional colors; this will permit exploration of sourcing and compositional differences via multivariate data analysis using both single technique and fused spectral data sets. Future work also could include quantitative EDXRF studies and the use of additional portable instruments at the site such as laser-induced breakdown spectroscopy. Both would aid in provenancing.

Acknowledgements M.K. Donais, D. Sparks, M. Redente, and D. George would like to thank the following individuals and organizations whose support contributed to the work in this paper: the Institute for Mediterranean Studies; the Soprintendenza per I Beni Archeologici dell'Umbria; the Parco Archaeologico e Ambientale dell'Orvietano; and Dr. Claudio Bizzarri. J. Van Pevenage and P. Vandenabeele would like to thank Sylvia Lycke for her help and support during the measurements.

References

1. D. Brems, P. Degryse, Trace Element Analysis in Provenancing Roman Glass-Making. Archaeom. **56**, 116 (2014)
2. C.M. Jackson, S. Paynter, A Great Big Melting Pot: exploring Patterns of Glass Supply, Consumption and Recycling in Roman Coppergate, York. Archaeom. **58**, 68 (2016)
3. E. Neri, M. Verità, I. Biron, M.F. Guerra, Glass and gold: analyses of 4th–12th centuries Levantine mosaic tesserae. A contribution to technological and chronological knowledge. J Arch. Sci. **70**, 158 (2016)
4. T. Rehren, I.C. Freestone, Ancient glass: from kaleidoscope to crystal ball. J. Arch. Sci. **56**, 233 (2015)
5. C. Moretti and S. Hreglich, *Raw Materials, Recipes and Procedures Used for Glass Making* in Modern Methods for Analysing Archaeological and Historical Glass, ed. By K. Janssens (John Wiley & Sons Ltd.: West Sussex, United Kingdom, 2013), pp. 23-47
6. I. Biron and M.-H. Chopinet, *Colouring, Decolouring and Opacifying of Glass* in Modern Methods for Analyzing Archaeological and Historical Glass, ed. By K. Janssens (John Wiley & Sons Ltd.: West Sussex, United Kingdom, 2013), pp. 49-65
7. S. Cagno, P. Cosyns, A. Izmer, F. Vanhaecke, K. Nys, K. Janssens, Deeply colored and black-appearing Roman glass: a continued research. J. Arch. Sci. **42**, 128 (2014)
8. A. Aerts, K. Janssens, F. Adams, H. Wouters, Trace-level Microanalysis of Roman Glass from Khirbet, Qumran, Israel. J. Archaeol. Sci. **26**, 883 (1999)
9. Y. Abe, R. Harimoto, T. Kikugawa, K. Yazawa, A. Nishisaka, N. Kawai, S. Yoshimura, I. Nakai, Transition in the use of cobalt-blue colorant in the New Kingdom of Egypt. J. Arch. Sci. **39**, 1793 (2012)
10. B. Dal Bianco, U. Russo, Basilica of San Marco (Venice, Italy/Byzantine period): nondestructive investigation on the glass Mosaic Tesserae. J. Non-Cryst. Solids **358**, 368 (2012)
11. M. Tite, O. Watson, T. Pradell, M. Matin, G. Molina, K. Domoney, A. Bouquillon, Revisiting the beginnings of tin-opacified Islamic glazes. J. Arch. Sci. **57**, 80 (2015)
12. A. Rousaki, A. Coccato, C. Verhaeghe, B.-O. Clist, K. Bostoen, P. Vandenabeele, L. Moens, Combined Spectroscopic Analysis of Beads from the Tombs of Kindoki, Lower Congo Province (Democratic Republic of the Congo). Appl. Spectrosc. **70**, 76 (2016)
13. P. Ricciardi, P. Colomban, A. Tournié, V. Milande, Nondestructive on-site identification of ancient glasses: genuine artefacts, embellished pieces or forgeries? J. Raman Spectrosc. **40**, 604 (2009)
14. A.K. Carter, L. Dussubieux, N. Beavan, Glass Beads from 15th–17th Century CE Jar Burial Sites in Cambodia's Cardamom Mountains. Archaeom. **58**, 401 (2016)
15. M. Smirniou, T. Rehren, Shades of blue – cobalt-copper coloured blue glass from New Kingdom Egypt and the Mycenaean world: a matter of production or colourant source? J. Arch. Sci. **40**, 4731 (2013)
16. A. Silvestri, S. Tonietto, G. Molin, and P. Guerriero, The palaeo-Christian glass mosaic of St. Prosdocimus (Padova, Italy): Archaeometric characterisation of tesserae with copper- or tin-based opacifiers, J. Arch. Sci., (2013)
17. T. Palomar, M. Oujja, M. García-Heras, M.A. Villegas, M. Castillejo, Laser induced breakdown spectroscopy for analysis and characterization of degradation pathologies of Roman glasses. Spectrochim. Acta B **87**, 114 (2013)
18. M. Oujia, M. Sanz, F. Agua, J.F. Conde, M. Garcia-Heras, A. Davila, P. Onate, J. Sanguino, J.R. Vazquez de Aldana, P. Moreno, M.A. Villegas, M. Castellijo, Multianalytical characterization of Late Roman glasses including nanosecond and femtosecond laser induced breakdown spectroscopy. J. of Anal. At. Spectrom. **30**, 1590 (2015)
19. D. Rosenow, T. Rehren, Herding cats - Roman to Late Antique glass groups from Bubastis, northern Egypt. J. Arch. Sci. **49**, 170 (2014)
20. P. Vandenabeele, M.K. Donais, Mobile Spectroscopic Instrumentation in Archaeometry Research. Appl. Spectrosc. **70**, 27 (2016)
21. M.K. Donais, B. Duncan, D. George, C. Bizzarri, Comparisons of Ancient Mortars and Hydraulic Cements through In-Situ Analyses by Portable X-Ray Fluorescence Spectrometry. X-Ray Spectrom. **39**, 146 (2010)
22. M.K. Donais, B. Duncan, S. Wojtas, A. Desmond, D. George, Differentiation of Hypocaust and Floor Tiles at Coriglia, Castel Viscardo (Umbria, Italy) using Principal Component Analysis (PCA) and Portable X-Ray Fluorescence (XRF) Spectrometry. Appl. Spectrosc. **66**, 1005 (2012)
23. M.K. Donais, D. George, S. Roberts, J. Roberts, E. Wu, *Analyses of Ancient Roman Pigments by Portable X-Ray Fluorescence and Raman Spectroscopies, in Conference of the Federation of Analytical Chemistry and Spectroscopy Societies* (Louisville, Kentucky, 2009)
24. D.B. George, *In dagini archeologiche presso la Fontana di Coriglia* in Da Orvieto a Bolsena Percorsi nella Storia un Territorio tra Etruschi e Romani, ed. By G.M.D. Fina (Pacini Editore: Pisa, 2013), pp. 82-88
25. D. Sokaras, A.G. Karydas, A. Oikonomou, N. Zacharias, K. Beltsios, V. Kantarelou, Combined elemental analysis of ancient glass beads by means of ion beam, portable XRF, and EPMA techniques. Anal. Bioanal. Chem. **395**, 2199 (2009)
26. K. Tantrakarn, N. Kato, A. Hokura, I. Nakai, Y. Fujii, S. Gluscevic, Archaeological analysis of Roman glass excavated from Zadar, Croatia, by a newly developed portable XRF spectrometer for glass. X-Ray Spectrom. **38**, 121 (2009)
27. A.M. Pollard and C. Heron, *The Chemistry, Corrosion and Provenance of Archaeological Glass* in Archaeological Chemistry, ed. By (The Royal Society of Chemistry: London, 2008), pp. 144-192

28. M.K. Donais, M. Redente, D. George, Field Research and Experiential Learning with Undergraduates: investigations of Roman Glass Tesserae by Portable X-Ray Fluorescence Spectroscopy. Spectrosc. **29**, 28 (2014)
29. P. Croveri, I. Fragala, E. Ciliberto, Analysis of glass tesserae from the mosaics of the "Villa del Casale" near Piazza Armerina (Enna, Italy). Chemical composition, state of preservation and production technology. Appl. Phys. A Mater. Sci. Process. **100**, 927 (2010)
30. N.Q. Liem, G. Sagon, V.X. Quang, H. Van Tan, P. Colomban, Raman study of the microstructure, composition and processing of ancient Vietnamese (proto) porcelains and celadons (13–16th centuries). J. Raman Spectrosc. **31**, 933 (2000)
31. E. Basso, C. Invernizzi, M. Malagodi, M.F. La Russa, D. Bersani, P.P. Lottici, Characterization of colorants and opacifiers in roman glass mosaic tesserae through spectroscopic and spectrometric techniques. J. Raman Spectrosc. **45**, 238 (2014)
32. P. Ricciardi, P. Colomban, A. Tournié, M. Macchiarola, N. Ayed, A non-invasive study of Roman Age mosaic glass tesserae by means of Raman spectroscopy. J. Archaeol. Sci. **36**, 2551 (2009)
33. M. Sendova, V. Zhelyaskov, M. Scalera, M. Ramsey, Micro-Raman spectroscopic study of pottery fragments from the Lapatsa tomb, Cyprus, ca 2500BC. J. Raman Spectrosc. **36**, 829 (2008)
34. J. van de Weerd, G.D. Smith, S. Firth, R.J.H. Clark, Identification of black pigments on prehistoric Southwest American potsherds by infrared and Raman microscopy. J. Archaeol. Sci. **31**, 1429 (2004)
35. S. Akyuz, T. Akyuz, S. Basaran, C. Bolcal, A. Gulec, Analysis of ancient potteries using FT-IR, micro-Raman and EDXRF spectrometry. Vib. Spectrosc. **48**, 276 (2008)
36. F. Bordignon, P. Postorino, P. Dore, G.F. Guidi, G. Trojsi, V. Bellelli, In search of Etruscan colours: a spectroscopic study of a painted terracotta slab from Ceri. Archaeom. **49**, 87 (2007)
37. M. a Legodi and D. de Waal, Raman spectroscopic study of ancient South African domestic clay pottery, J. Raman Spectrosco. **45**, 238 (2007)
38. S. Lahlil, M. Cotte, I. Biron, J. Szlachetko, N. Menguy, J. Susini, Synthesizing lead antimonate in ancient and modern opaque glass. J. Anal. Atom. Spectrom. **26**, 1040 (2011)
39. I.C. Freestone, *Composition and Microstructure of Early Opaque Red Glass* in Early Vitreous Materials, ed. By M. Bimson and I.C. Freestone (British Museum, 1987), pp. 173-191
40. C. Boschetti, J. Henderson, J. Evans, C. Leonelli, Mosaic tesserae from Italy and the production of Mediterranean coloured glass (4rd century BCE–4th century CE). Part I: Chemical composition and technology, Journal of Archaeological Science: Reports **7**, 303 (2016)
41. P. Colomban, H.D. Schreiber, Raman signature modification induced by copper nanoparticles in silicate glass. J. Raman Spectrosco. **36**, 884 (2005)
42. P. Colomban, A. Tournie, P. Ricciardi, Raman spectroscopy of copper nanoparticle-containing glass matrices: ancient red stained-glass windows. J. Raman Spectrosco. **40**, 1949 (2009)
43. J. Zuo, X.C. Zhao, R. Wu, G.F. Du, C.Y. Xu, C.S. Wang, Analysis of the pigments on painted pottery figurines from the Han Dynasty's Yangling Tombs by Raman microscopy. J. Raman Spectrosc. **34**, 121 (2003)
44. S. Cagno, P. Cosyns, K. Nys, and K. Janssens, *Black-Appearing Roman Glass* in Modern Methods for Analyzing Archaeological and Historical Glass, ed. By K. Janssens (John Wiley & Sons Ltd.: West Sussex, United Kingdom, 2013), pp. 369-385
45. L.C. Prinsloo, W. Barnard, I. Meiklejohn, K. Hall, The first Raman spectroscopic study of San rock art in the Ukhahlamba Drakensberg Park, South Africa. J. Raman Spectrosc. **39**, 646 (2008)
46. L.C. Prinsloo, P. Colomban, A Raman Spectroscopic Study of the Mapungubwe Oblates: glass Trade Beads Excavated at n Iron Age Archaeological Site in South Africa. J. Raman Spectrosco. **31**, 79 (2011)
47. L.C. Prinsloo, A. Tournié, P. Colomban, A Raman Spectroscopic Study of Glass Trade Beads Excavated at Mapungubwe Hill and K2, Two Archaeological Sites in Southern Africa, Raises Questions about the Last Occupation Date of the Hill. J. Archaeol. Sci. **38**, 3264 (2008)
48. L.C. Prinsloo, P. Colomban, A Raman spectroscopic study of the Mapungubwe oblates: glass trade beads excavated at an Iron Age archaeological site in South Africa. J. Raman Spectrosco. **39**, 79 (2008)
49. P. Colomban, G. March, L. Mazerolles, T. Karmous, N. Ayed, A. Ennabli, H. Slim, Raman identification of materials used for jewellery and mosaics in Ifriqiya. J. Raman Spectrosc. **34**, 205 (2003)
50. A. Moropoulou, N. Zacharias, E.T. Delegou, B. Maróti, Z. Kasztovszky, Analytical and technological examination of glass tesserae from Hagia Sophia. Microchem. J. **125**, 170 (2016)
51. C.M. Jackson, D. Greenfield, L.A. Howie, An Assessment of Compositional and Morphological Changes in Model Archaeological Glasses in an Acid Burial Matrix. Archaeom. **54**, 489 (2012)
52. R. Bertoncello, L. Milanese, U. Russo, D. Pedron, P. Guerriero, S. Barison, Chemistry of cultural glasses: the early medieval glasses of Monselice's hill (Padova, Italy). J. Non-Cryst. Solids **306**, 249 (2002)
53. K. Janssens, B. Vekemans, L. Vincze, F. Adams, A. Rindby, A micro-XRF spectrometer based on a rotating anode generator and capillary optics, spectrochim Acta. Part B **51**, 1661 (1996)
54. M. Tite, T. Pradell, A.J. Shortland, Discover, production and use of tin-based opacifiers in glasses, enamels and glazes from the late Iron Age onwards: a reassessment. Archaeom. **50**, 67 (2008)